Improved Mapping of Long-Term Forest Disturbance and Recovery Dynamics in the Subtropical China Using All Available Landsat Time-Series Imagery on Google Earth Engine Platform

Jianwen Hua, Guangsheng Chen, Lin Yu, Qing Ye, Hongbo Jiao, and Xifang Luo

***Abstract*—After implementations of many economic and forestry policies during recent 30 years, forest cover in China has experienced significant changes. The fine scale and long-term information on forest temporary (disturbance) loss, persistent loss (deforestation), and gains (afforestation/reforestation) will provide a guide for forest management and policies at regional scale. Using Jiangxi Province as a pilot study region, here we assessed forest cover dynamics in the subtropical China during 1986–2019 by integrating time-series Landsat images, Landsat-based Detection of Trends in Disturbance and Recovery algorithm and Random Forest classifier on the Google Earth Engine Platform. The accuracy assessment indicated a high overall accuracy (>90%) and Kappa coefficient (>0.9) for both forest gain and loss detections as evaluated against various sources of plot-level sample data and the existing global forest change product. The total forest loss area was 18 697.79 km^2, with persistent loss area of 3394.31 km^2 due to land conversion during 1986–2019, while persistent (net) forest gain area was 45 656.96 km^2, accounting for 57.70% of the forest area in 1986. Forest loss area exhibited large interannual variations, but showed a general increase trend from 1986 to 2019. The annual variation patterns of forest gain and loss area were associated with the changes in forestry policies and large disturbance events. Our assessments on the long-term and fine scale forest dynamic patterns will help evaluate the effectiveness of forest management practices and forestry polices on forest resource sustainability, and climate change and greenhouse gases mitigation in Jiangxi Province and China.**

***Index Terms*—Forest dynamics, forest gain, forest loss, forest management, Landsat-based Detection of Trends in Disturbance and Recovery (LandTrendr), random forest (RF).**

Manuscript received November 13, 2020; revised January 7, 2021; accepted January 30, 2021. Date of publication February 10, 2021; date of current version March 10, 2021. This work was supported in part by the Natural Science Foundation of Zhejiang Province under Grant LY20C030001, in part by the Scientific Research Foundation of Zhejiang A&F University under Grant 2034020080, and in part by the 111 Project under Grant D18008. (*Corresponding author: Guangsheng Chen.*)

Jianwen Hua and Guangsheng Chen are with the State Key Laboratory of Subtropical Silviculture, Zhejiang A&F University, Hangzhou 311300, China, and also with the College of Environmental and Resource Sciences, Zhejiang A&F University, Hangzhou 311300, China (e-mail: 2366583937@qq.com; auburncgs@126.com).

Lin Yu is with the Bureau of Agriculture and Rural Affairs of Lin'An District, Hangzhou 311300, China (e-mail: 411851186@qq.com).

Qing Ye is with the College of Forestry, Jiangxi Agricultural University, Nanchang 330045, China (e-mail: yeqing@jxau.edu.cn).

Hongbo Jiao is with the Forestry Industry Development Administration, Xinyu 338000, China (e-mail: xycyhgk@163.com).

Xifang Luo is with the East China Forest Inventory and Planning Institute of National Forestry and Grassland Administration, Hangzhou 310019, China (e-mail: luoxfhdy@126.com).

Digital Object Identifier 10.1109/JSTARS.2021.3058421

I. Introduction

FORESTS play a vital role in environmental improvement, landscape aesthetics, the mitigation of climate change, and determination of energy budgets [1]. Due to increasing forest cover and relatively young forest age [2]–[5], forests in China were an important carbon sink [6]–[9] and played an important role in the global carbon budget [10], [11]. However, it is still uncertain about the contributions from forest disturbance and management because of the lack of a long-term and high spatial and temporal accuracy dataset for forest dynamics. During the past 50 years, forest structure and function in China have been significantly changed due to enhancing and varying degrees of disturbance events, including natural (e.g., climate extremes, hurricane, insects and pests outbreak, and fire burning) and human disturbance (e.g., harvesting and land use change), and the forest recovery after disturbance [12]–[14]. For example, climate extremes of freezing disasters have caused large area of forest damage in the subtropical China in 2008 [15]; the affected forest area by insect and diseases has increased from about 1 million ha in 1950 to 11 million ha in 1990 and to 11.6 million ha in 2010, which accounts for about 6% of China's forest land area [16]. In addition, China has put forward many forestry policies and regulations, such as forest right reform, timberland base shifting, "green for grain" program, and natural forest conservation program (NFCP), and has also implemented many national and regional afforestation/reforestation projects, such as the Three-North Shelterbelt Project in the northern, northeastern, and northwestern China (1978), and the Shelterbelts Project along the Upper and Middle Reaches of the Yangtze River (1989), to promote forest quantity and quality and in the meanwhile meet the demand of timber and pulpwood in China [2], [15]–[17], which further significantly altered the forest structure and functions. Therefore, knowledge of spatiotemporally explicit forest cover dynamics is important for understanding forest carbon cycle in China.

Since the United States Geological Survey (USGS) opened Landsat data for free access, the change detection algorithms

for forest losses have been developed rapidly based on the long-term Landsat time-series stacks (LTSS), such as VCT (vegetation change tracker), LandTrendr (Landsat-based Detection of Trends in Disturbance and Recovery), and BFAST (Breaks For Additive Season and Trend Monitor) algorithms [18]–[23]. The LandTrendr algorithm fits the spectral indices of each pixel in the time series and selects the most suitable regression model to segment the time series through the *P*-value test of the *F* distribution, and extracts the change trend of the indices in the time series [19]. The algorithm only requires one or two years to input a cloudless image or multiple cloud-covered images, and it can not only capture the long-term slow change trend of forests but also detect the mutation trend, and thus has a good applicability worldwide [14], [24]–[28]. Another factor that affects change detection is the choice of input variables. Different bands, vegetation indices (VIs), image conversion processing, and subpixel variables are used in many previous studies [29], [30]. For example, the short-wave infrared band (SWIR) from Landsat images is sensitive to moisture conditions, so it has been successfully used for detecting disturbance [31]. However, single band is susceptible to some external environmental factors such as terrain factors and atmospheric conditions. In contrast, VIs can reduce these effects [30]. VIs such as NDVI (normalized difference vegetation index), NDWI (normalized difference water index), NBR (normalized burned ratio), and Tasselled cap brightness (TCB), greenness (TCG), and wetness (TCW) are widely used [32]–[35].

A few studies have addressed forest dynamics represented by gain and loss at county-level scale based on LandTrendr, VCT, or other change detection algorithms in China. For example, Diao *et al.* [36] assessed the changes of forest age in Lishui County of Zhejiang Province during 1987–2017 by combining the VCT and Random Forest (RF) algorithms; Shen *et al.* [13] studied the forest disturbance and recovery in Fogang County of Guangdong Province based on Landsat images and VCT algorithms; Zhang [37] and Zhong *et al.* [14] estimated the forest losses in Changting County of Fujian Province based on Landsat image series and LandTrendr; Guo [38] estimated the forest dynamics and its impacts in the northeastern China based on MODIS products and a landscape model; Fang *et al.* [39] explored forest disturbance history and its impacts on forest biomass in Huitong County of Hunan Province during 1986–2016 based on Landsat images and VCT algorithms (combining allometry and Landsat-derived disturbance history to estimate tree biomass in subtropical planted forests); Liu *et al.* [27] examined the forest disturbance and recovery in the eastern coastal area of Zhejiang Province based on Landsat images and LandTrendr algorithms. These studies addressed the forest changes at relatively small scale. In addition, the global forest change (GFC) products [40] have also estimated the national and regional forest loss and gain based on the classification of Landsat image series during 2001–2019; however, this product has not been specifically validated based on local forest state data [41], especially the plot-level inventory data in China. In addition, this product only covered the recent 20 years and lack of the earlier period (i.e., 1980–2000) when China has experienced stronger disturbance and more rapid changes in forest cover. Therefore, similar to the national forest disturbance and recovery data products for the United States [18], [42], it is also necessary to develop an accurate middle spatial resolution (e.g., 30 m) forest loss, gain, and resultant age structure products for China at regional or national scale based on a longer period of Landsat images and effective validation and training using more intensive local observational data.

The forest coverage of Jiangxi Province in the subtropical China is 61.16% in 2014–2018 according to the ninth national forest resource inventory (NFRI) ranking as the second place in China. In addition, this region has experienced rapid changes in forest gains and losses due to afforestation/reforestation, intensive management, and disturbance. Although most forest harvesting areas were preplanned and approved by the local forest departments under the permissions of national and local forest laws and regulations; however, many activities, such as the household cutting of trees and small-scale unplanned or illegal logging especially in private forest properties, occurred frequently and have significantly affected the forest structure and function in this province [43]. Although the provincial and national governments have continuously conducted forest surveys every five years and provided forest resource reports, the forest dynamics due to scattered and short-term disturbance events cannot be effectively and accurately monitored. Therefore, the goal of this article is to assess the forest cover dynamics (both temporary and persistent loss and gain) for Jiangxi Province from 1986 to 2019 through synthesizing the Landsat image series and various sources of observational data using an integrative approach of the LandTrendr algorithms and RF secondary classification in the Google Earth Engine (GEE) platform. Specifically, our study objectives are to 1) recalibrate the LandTrendr change detection algorithms and develop effective indices based on the intensive plot-level inventory data in Jiangxi Province; 2) estimate forest loss and gain area and their spatial and temporal change patterns during 1986–2019; 3) and discuss the effects of forest management and disturbance events. Using Jiangxi Province as a pilot study area, our ultimate research goal is to develop a national scale forest disturbance and recovery dataset for China in the near future, and provide a relatively more accurate spatiotemporal forest disturbance and recovery dataset for the uses in the assessments of forest resources, global change impacts, and greenhouse gas emissions.

II. Methods

A. Study Region

The study area is the entire Jiangxi Province (between 24°07′–29°09′N and 114°02′–117°97′E), which is located in the subtropical China on the south of the middle and lower reaches of the Yangtze River (Fig. 1). This region belongs to a typical subtropical monsoon climate, characterized by humid and hot summer and dry and warm winter, which is favorable for forest growth. The average annual temperature is ranged between 16.3 and 19.5 °C, generally increases from the north to the south. The mean annual rainfall ranges between 1341 and 1940 mm, with 80% falling in the growing season. The main terrain is hilly and mountainous and the major soil type is red soil [44]. The

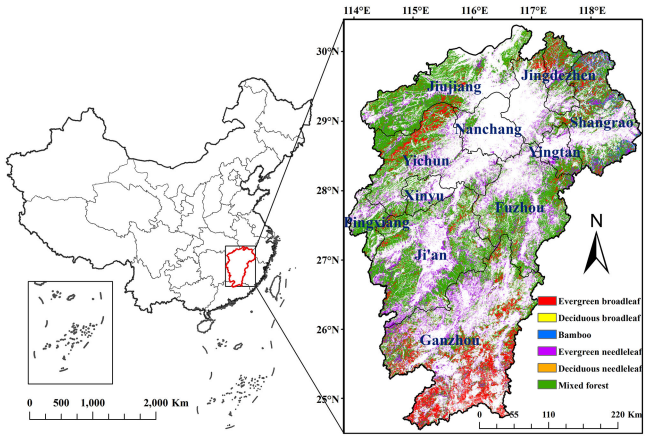

Fig. 1. Location of Jiangxi Province and the main forest types in 2010 (Data source: [47]).

main forest types include evergreen broadleaf forest, evergreen needleleaf forest, and mixed forest. The main broadleaf tree species include *Cinnamomum camphora* (L.) Presl., *Phoebe zhennan* S. Lee, and *Magnolia denudata* Desr.; the main needleleaf tree species include *Pinus massoniana* (Chinese red pine), *Cunninghamia lanceolata* (Chinese fir), and *Metasequoia glyptostroboides* [45], [46]. The forest coverage in Jiangxi Province has increased from 36.70% during the first NFRI (1973–1976) to 61.16% during the ninth NFRI (2014–2018), ranking the second highest among all provinces in China. Forests in this region have also been extensively disturbed by various natural or human disturbance events and management activities. Major disturbance events include harvesting, insects, and diseases (e.g., pine wood nematode disease and long-horned beetle) and fire [46].

B. Work Flow

To achieve the objectives, this article was conducted through following work flows in Fig. 2. The main flows include 1) data collection including training and validation data, and Landsat images; 2) masking out the persistent nonforest and calculations of the variables for inputs in the LandTrendr algorithms and RF model; 3) implementations of the LandTrendr and RF model to obtain preliminary results for forest gain and loss; 4) postprocessing based on the preliminary forest gain and loss products; 5) validations for the derived forest gain and loss products; and 6) producing and analyzing the final products.

C. Descriptions of Training and Validation Sample Data

To train the RF algorithms and validate the derived results, we collected a lot of sample plots, which were from three sources including NFRI, LFMI (local forest management inventory plots) and GEVI (Google Earth based visual interpretation plots) (Fig. 3; Table I). NFRI is conducted every five years at national scale. The NFRI sets up over hundreds of thousands of permanent sample plots, varying in different inventory time periods, for example, 0.415 million plots during the seventh inventory (2004–2008). The area of sample plots ranges from

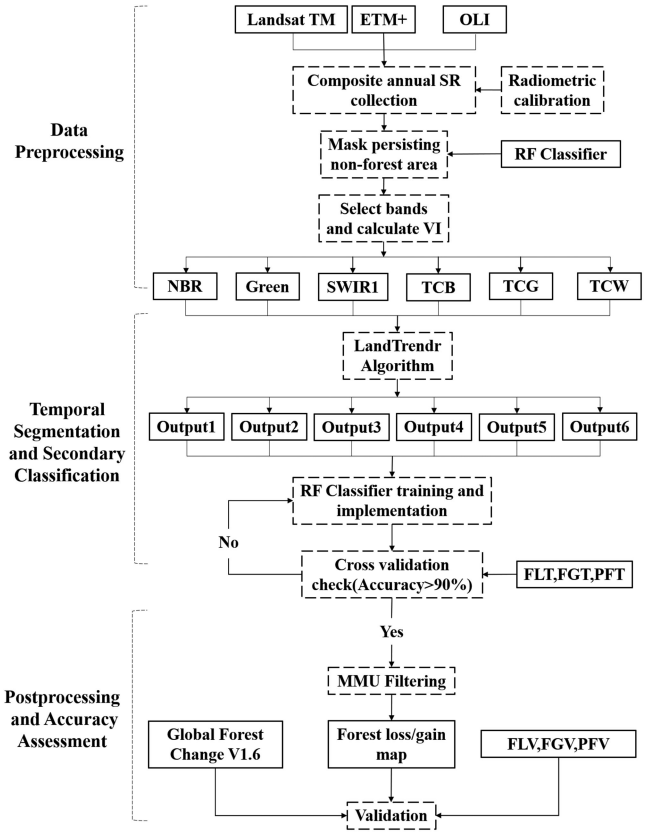

Fig. 2. Work flow and logics in this article. Note: NBR, TCB, TCG, and TCW are vegetation indices. Green: green band; SWRI1: short-wavelength infrared band 1; RF: random forest classifier; FLT: forest loss training data; FGT: forest gain training data; PFT: persistent forest training data; FLV: forest loss validation data; FGV: forest gain validation data; PFV: persistent forest validation data.

TABLE I
CHARACTERISTICS OF THE COLLECTED VARIOUS SAMPLING PLOT DATA

Categories	NFRI	LFMI (Jingdezhen)	LFMI (Longnan)	LFMI (Yihuang)	GEVI
FGV	4	28	19	20	60
FGT	14	83	59	56	87
FLV	6	37	18	18	60
FLT	13	111	57	49	95
PFV	43	19	17	21	35
PFT	24	17	18	23	49
Total	104	295	188	187	386

Note: NFRI: national forest resource inventory; LFMI: local forest management inventory; GEVI: Google Earth based Visual Interpretation; PFT: persistent forest training plots; PFV: persistent forest validation plots; FLT: forest loss training plots; FLV: forest loss validation plots; FGT: forest gain training plots; FGV: forest gain validation plots.

667 to 800 m^2. Among these samples, a few plots have recorded the clearcut (loss) events during each five-year period. Based on these plots, the NFRI reports provide a rough estimation on the total clearcut area at provincial and national scales. Due to data confidentiality, we can only obtain the data during the sixth NFRI (1999–2003). There are totally 1118 forest sample plots for Jiangxi Province and the total sample plots for forest loss and gain are 464 and 430, respectively, during this period. LFMI is generally conducted at county level and the purpose

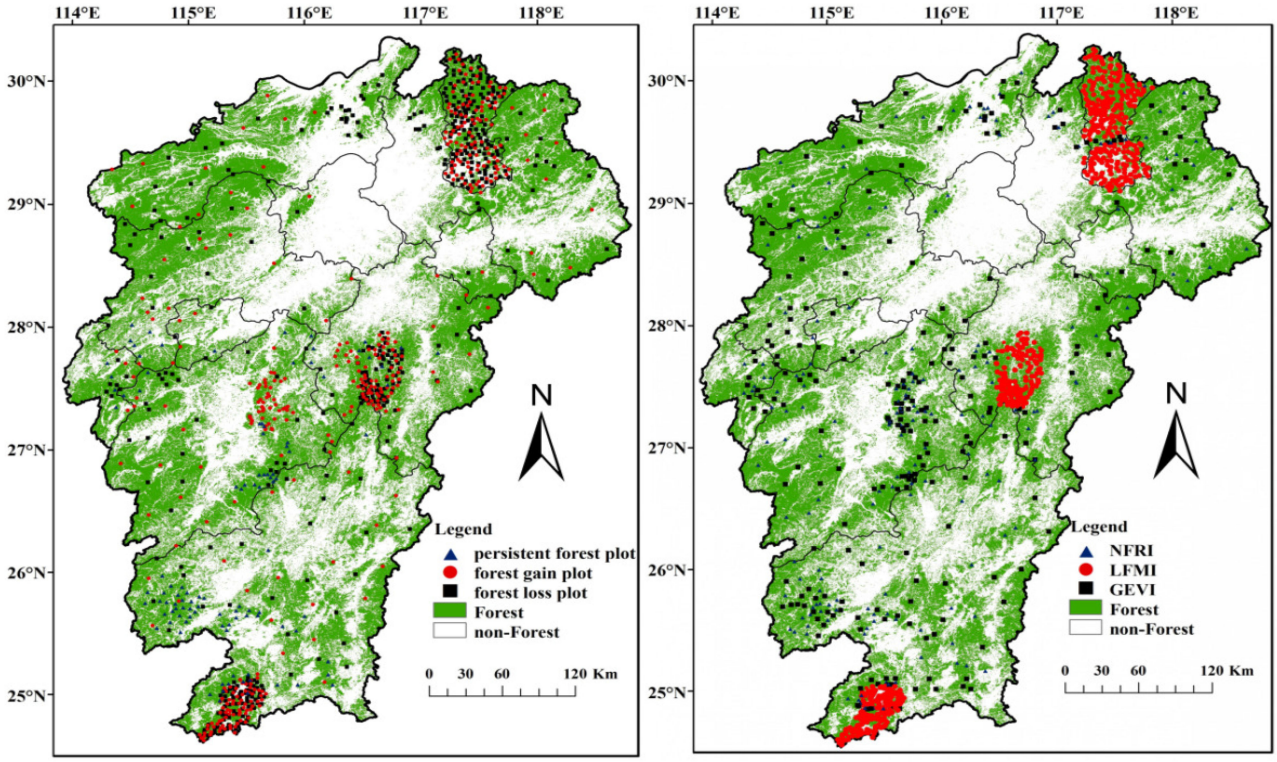

Fig. 3. Roles, data sources, and locations of the sample plots for the training and validations of forest gain and loss classifications. NFRI: National Forest Resource Inventory; LMFI: Local Forest Management Inventory; GEVI: Google Earth Visual Interpretation. Note: the points represent the center of each polygon or sample plot and the grid cells at the center are used to train and validate.

is to better manage local forest resources. Compared with the NFRI, LFMI generally more widely investigates the forest areas within each county using a whole subcompartment forest stand (i.e., a relatively uniform forest stand) as an investigation unit, so the area of plots is different but forest community is uniform within each plot. The records in LFMI for some forest stand properties (e.g., age, tree height, and diameter at breast height) have been often criticized for not accurate enough; however, the recorded forest gain and loss locations are accurate enough for the training and evaluations of classification results. We obtained the LFMI data for Jingdezhen City (including data from 2008–2019), Longnan County (2009–2013), and Yihuang County (2009–2019) (Table I). To increase the representatives, in addition to abovementioned samples, we also identified many sample plots based on available high-resolution ($<$1 m) images in Google Earth system using visual interpretation method. These samples are generally selected in the large-scale deforested or afforested/reforested areas (at least 30 $\times$ 30 m area) and can be easily identified directly by eyes based on our long-term classification experience. The identified sample plots are distributed within years 2010–2016 and widely distributed across Jiangxi Province. Totally, 386 sample plots are obtained through the GEVI method. The central grid cell within each sample plot was used to train or validate classification results.

The locations of various types (NFRI, LFMI, and GEVI) of sample plots were listed in Fig. 3 and their characteristics were listed in Table I. The samples (total number 1160) are divided into six categories: persistent forest training samples (PFT), persistent forest validation samples (PFV), forest loss training samples (FLT), forest loss validation samples, forest gain training samples (FGT), and forest gain validation samples. The collected information at these plots included the coordinates at the center of each plot, forest cover change categories (loss, gain, or persistent forest), the year in which forest loss or gain occurred, and the plot boundary and area. To increase the accuracy for training and validation, only the grid cells at the center of each plot rather than the entire plot were selected. These plot data were used to train the RF classification models and accuracy evaluation for results.

Except for abovementioned sample plots, we have also collected the gridded GFC product (v1.7; [40]) to compare our classification results. The GFC product recorded forest gain and loss based on the classifications of time series Landsat images at 30 m spatial resolution during 2001–2019.

D. Time Series Landsat Images and Preprocessing

The Landsat images are originally sourced from the USGS[1]. We used the GEE[2] platform to select and preprocess the time series Landsat images. The GEE platform, using state-of-the-art cloud-computing and storage capabilities, has archived a large catalog of earth observation data and enabled the scientific community to work on petabytes of satellite imagery rapidly

[1][Online]. Available: https://landsat.usgs.gov/landsat-surface-reflectance-data-products

[2][Online]. Available: https://earthengine.google.com/

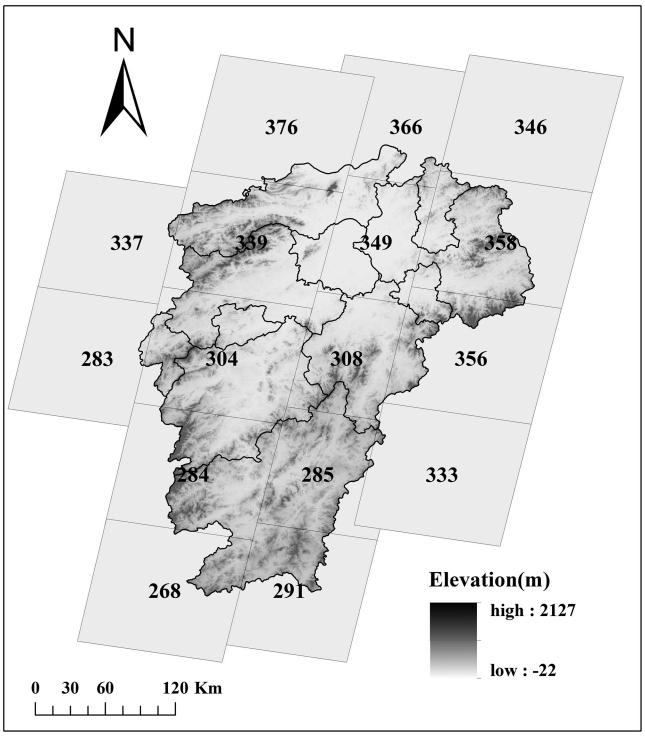

Fig. 4. Elevation (m) and paths and rows of Landsat time series image scenes that cover Jiangxi Province.

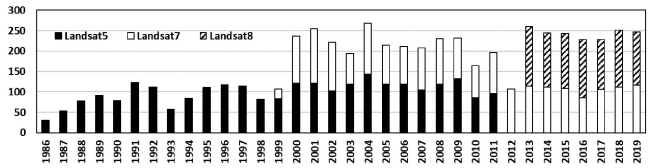

Fig. 5. Collected Landsat image numbers from different sensors during 1986–2019 for Jiangxi Province.

using parallel processing [40]. This article collected all available Landsat images from May to October during 1986–2019 for Jiangxi Province. It needs totally 16 scenes of Landsat images to cover the entire study region (Fig. 4).

To minimize miss-registration errors and to provide radiometric consistency, only LEDAPS (Landsat Ecosystem Disturbance Adaptive Processing System) surface reflectance data (subpixel accuracy), provided by the USGS climate data record [48], were used. This dataset has already atmospherically corrected using LEDAPS or LaSRC (surface reflectance code) [49]. Both algorithms used CFMASK as a built-in cloud detection method and generated quality assessment bands which identify the pixels that exhibit adverse instrument, atmospheric, or surficial conditions [50]. We removed the pixels marked as cloud or other improper objects and fill them with clear pixels of other neighboring months to ensure that only cloud-free images were generated to construct LTSS. In order to reduce the error caused by different Landsat sensors, we used the slope and intercept approach to match the Landsat8 bands and Landsat5 & 7 bands [51]. Fig. 5 showed the total image numbers collected in each year during 1986–2019. These images were from the sensors of Landsat5, Landsat7, and Landsat8.

E. Mask of Persistent Nonforest Cover

The crop and grass planting and harvesting events could be easily classified as the forest gain and loss signals, thus potentially impose classification errors to the determinations of forest gain and loss areas. Before the implementation of LandTrendr algorithms, the persistent nonforest areas in 1986 and 2019 were classified using the RF classifier and the sample data from the NFRI in 1989–1993 (to represent 1986), as well as the GEVI and LFMI data during the recent 10 years (to represent 2019). The persistent nonforest cover maps were then applied to screen out nonforest areas in Jiangxi Province in both years.

F. LandTrendr Algorithm for Maximum Change Magnitude Detections

The images after preprocessing were normalized and image stack was created, and then the stack was arranged for trajectory segmentation. The LandTrendr time segmentation algorithm has been regarded as one of the best approaches to effectively detect forest disturbance and recovery [19], [52]. Through the extraction of the surface reflectance change trend from the time-series data, the LandTrendr algorithm can capture short-term disturbance and long-term recovery trend [19]. Temporal segmentation is the core approach of the algorithm to capture both abrupt and slow phenomena in the Landsat time series. The implementation of LandTrendr segmentation algorithm includes six steps [19]. The first step is the removal of spikes (residual clouds, snow, smoke, or shadows). A despiking algorithm in LandTrendr is applied, and this despiking process is iterative, correcting the worst spike each time. The second step is the identification of potential vertices. A vertex in the time series is the [year, spectral/band value] combination which divides the two distinct period (before and after the vertex). The regression-based vertex identification strategy is used to identify vertices. The excess segmentations are removed based on the angle criterion, and this process is iterated until the segmentation numbers equal to the *max-segments* parameter. The third step is the trajectories fitting. The vertex identification process is to identify the years of breaks in the time series, while the trajectory fitting process is to identify the y-axis (the spectral/band values) given the x-axis vertex points. This fitting process is actually a smoothing method to smooth the noises in trends but keeps the abrupt changes. The goodness of fit is reflected by the p-value of a standard F-test. The fitted trajectory in this step is actually the maximally complex segmentation model. The fourth step is the simplification of models. This is to repeatedly refit the trajectory models for segment numbers countdown from *max_segments* to 1. The fifth step identifies the best model based on the p-value of F-test. The final step filters the segments through comparing the segmentation trajectories with the long-term percent vegetative cover change rate. A user-defined threshold is set to determine whether the segment change in spectral/band value is "stable." When the segment change is lower than the threshold, the

TABLE II
BANDS AND THE COMPOSITE INDICES AND THEIR CALCULATION METHODS IN LANDTRENDR [41]

Spectral index/band	Formula
TCB	0.2043 * Blue + 0.4158 * Green + 0.5524 * Red + 0.5741 * NIR + 0.3124 * SWIR1 + 0.2303 * SWIR2
TCG	− 0.1603 * Blue + − 0.2819 * Green + − 0.4934 * Red + 0.7940 * NIR + − 0.0002 * SWIR1 + − 0.1446 * SWIR2
TCW	0.0315 * Blue + 0.2021 * Green + 0.3102 * Red + 0.1594 * NIR + − 0.6806 * SWIR1 + − 0.6109 * SWIR2
NBR	(NIR − SWIR2)/(NIR + SWIR2)
Green	Green
SWIR1	SWIR1

#Note: denote the reflectance of various bands of the Landsat sensors.

segment is recorded as stable; otherwise, the segments will be considered as noises.

Different spectral indices had varying capabilities for accurate detection of subtler disturbance signals, with the NDVI performing less effectively than NBR or tasseled cap wetness (TCW). LandTrendr operates on a single band or spectral index; however, it is likely that a single spectral index will be insufficient to adequately characterize forest disturbance and regrowth [53]. Cohen [41] demonstrated that use of a single algorithm with multiple indices may be a more economical approach to employing ensemble stacking for improved disturbance mapping. Hence, we implemented LandTrendr algorithm in a multiband and spectral indices approach. The LandTrendr API in GEE was implemented. In Cohen [41], 13 combinations of bands and indices were tested, and the best 6 combinations of bands and indices were tasseled cap index of greenness, brightness, and TCW NBR, green band, and SWIR1 (Table II). Therefore, we input the preprocessed LTSS data into the LandTrendr temporal segmentation algorithm, and calculated all these indices and bands using the same parameter values in Cohen *et al*. [41]. The running result was an array image with 4×N years' dimension. Each pixel has a series of segments. Considering that the actual forest rotation period and forest loss and gain often greatly modify the values of these indices or bands, we used five years as a time window to extract the maximum change magnitude (decrease or increase) of these indices or bands within the window. Then, we exported the data (greatest loss/gain in 1987–1992, 1992–1997, 1997–2002, 2002–2007, 2007–2012, 2012–2019) to GEE asset, and these segmentation data will be further used to determine the final forest gain/loss years.

Forest loss can be caused by land use change from forest to nonforest and temporary removal of trees due to disturbance (e.g., clearcut, fire, insect & disease), while forest gain can be caused by the land use change from nonforest to forest and regrowth from cleared forest land. Due to the recovery of forests from nonforest land or clearcut sites need a long period (e.g., $>=5$ years) and the segmentation window is five years, the detections of the forest gain area in 2016–2019 may be not accurate and misleading. Therefore, in this article, we only presented the forest gain detection period for 1986–2015.

G. Identifying Forest Loss and Gain Using Random Forest Secondary Classification Method

The above LandTrendr operation results obtained the year of detection, the previous values of the indices/bands, magnitude, and duration of the greatest changes in the bands or spectral indices of each pixel within the time windows. The results from NBR were used to determine the final products for forest gain and loss in most of previous studies based on LandTrendr algorithms [14], [19]. Totally, there were six outputs based on the six bands/indices from LandTrendr. However, not all detected loss and gain during the study period [41]. Therefore, we integrated the LandTrendr results from all runs as a multispectral ensemble and applied the RF classifier as the secondary classification model to further identify the forest loss and gain patterns [41].

Each band in the multispectral ensemble includes the year of detection, spectral indices/bands change magnitude, the duration of the segment and the previous value of the indices/bands. Thus, a total of 24 (6 indices × 4 variables) variables are input into the RF model for every time window. Some training plots from the FLT (represents loss), PFT (represents persistent forest), and FGT (represents gain) categories were randomly selected for the RF model training (Fig. 2). For the first time, we use 80% of the training plots to train the RF classifier. The remaining plots are used to evaluate the accuracy of RF outputs. When the accuracy is higher than 90%, all training plots will be used for training; otherwise adjust the parameters of the classifier (numberOfTrees and variablesPerSplit) until the accuracy meets the requirements. We implemented RF (numberOfTrees = 1000) in GEE platform, and other parameters were set as the default. We set RF into the classification mode by code "classifier.setOutputMode (Classification)." Our purpose was to more accurately find out which pixels have actually experienced loss or gain and in which years based on multispectral ensemble derived from the LandTrendr algorithms. The loss and gain processes generally have a greater degree of spectral change magnitude. In order to reduce the commission errors, we set a threshold (TCW >0.2) to filter some noises before running the RF classifier. The model outputs were labeled with the years of loss/gain or "no loss/no gain." After the implementation of the RF model for every time window, all the pixels were labeled with gain/loss occurrence years or "no loss/no gain."

H. Postprocessing and Validation

For many satellite-based map products, the initial data had many small patches that likely were errors resulting from difficulties in classifying mixed pixels, and other unidentified issues. Minimum mapping unit (MMU) filtering is a common approach for reducing such errors [54]. Considering high forest coverage in Jiangxi Province, we set four pixels (0.36 ha) as the MMU to perform the MMU filtering based on the forest loss/gain map, and then derived the final forest gain and loss product.

The final forest gain and loss product was validated against the randomly selected validation sample plot data (Fig. 2). The selected plot numbers for forest gain, loss, and PFVs were shown in Table I. The user, producer, overall accuracy, and Kappa Coefficient were used to assess the performance of the detections

TABLE III
CLASSIFICATION ACCURACY ASSESSMENT RESULTS BASED ON THE VALIDATION SAMPLE PLOTS AND GLOBAL FOREST CHANGE PRODUCT [40]

		Loss	Gain	Persistent	Producer Accuracy	User Accuracy	Overall Accuracy	Kappa
Sample plots	Loss	133	2	4	95.68%	97.79%		
	Gain	0	124	7	94.65%	92.54%	94.07%	0.91
	Persistent	3	8	124	91.85%	91.85%		
Global Forest Change	Loss	114	2	4	95.00%	93.44%		
	Gain	3	109	8	90.83%	88.62%	90.56%	0.86
	Persistent	5	12	103	85.83%	89.57%		

of forest loss and gain area and spatial distribution. The user accuracy is calculated as: correctly classified plots/total number of classified sites in a confusion matrix, the producer accuracy is calculated as correctly classified reference plots/total number of reference sites, while the overall accuracy is calculated as the number of correctly classified plots/total number of plots, which is an average representation of user and producer accuracies. The higher overall accuracy reflects the stronger robustness of the results. Another accuracy indicator is the Kappa Coefficient, which is a measure of how the classification results compare to values assigned by chance. If kappa coefficient equals to 0, there is no agreement between the classified image and the reference image. If kappa coefficient equals to 1, then the classified image and the ground truth image are totally identical [55].

III. RESULTS

A. Accuracy Assessment

Based on the validation sample plots and the GFC product, the classification accuracy assessments were conducted. Overall, the LandTrendr algorithm with RF secondary classification approach can effectively detect forest loss and gain in Jiangxi Province (Table III). Specifically, for the validations using sample plots, the producer and user's accuracies were 95.68% and 97.79%, respectively, for forest loss detections, and 94.65% and 92.54%, respectively, for forest gain detections, with an overall accuracy of 94.07% and Kappa coefficient of 0.91. In addition, our derived forest loss and gain patterns matched well with the GFC product, with a high overall accuracy (90.56%) and Kappa coefficient (0.86). The persistent forest plots include many pixels experienced recovery or disturbance. The segmentation information extracted by the LandTrendr algorithm was quite similar between those pixels and loss/gain pixels, which resulted in a slightly lower accuracy for the detections of persistent forests.

To more clearly look at the validation results, we further displayed the comparisons between observed and classified forest loss and gain at spatial scale using selected subregions as examples (Fig. 6). For forest loss detections [Fig. 6(a)–(c)], the LandTrendr algorithm can successfully identify the sudden declines of NBR in 2016, 2018, and 1993/2015 (twice losses), respectively, based on the trajectory of segmentations. The validation plots from GEVI were located within the detected forest loss polygons. Similarly, for forest gain detections [Fig. 6(d) and (e)], the LandTrendr algorithm can also successfully identify the sudden increases of NBR in 2014 and 2015, respectively, based on the trajectory of segmentations. The validation plots from GEVI were also located within the detected forest gain polygons. These indicated that our mechanisms can successfully detect the spatial distributions of forest loss and gain area in Jiangxi Province.

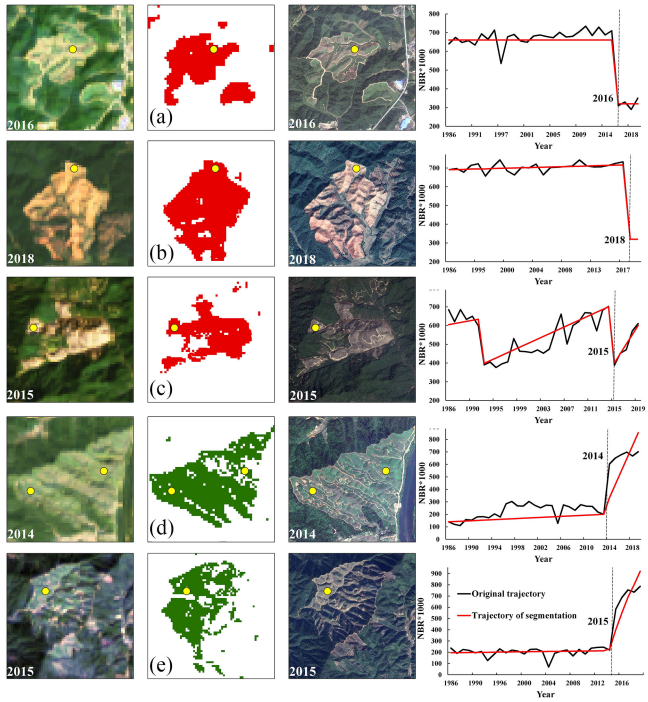

Fig. 6. Validation examples for the detected forest loss and gain patterns and the original and segmented trajectories based on the NBR index for selected regions [(a) Le'An County, Fuzhou City; (b) Guangchang County, Fuzhou City; (c) Zixi County, Fuzhou City; (d) Jingdezhen City; (e) Shangyou County, Ganzhou City] in Jiangxi Province. The graphs in the left column are Landsat images, in the middle column are classified forest loss/gain pixels (red colors denote loss area and green colors denote gain area), and in the right column are Google Earth high-resolution images.

B. Assessments of Temporal Changes in Forest Loss and Gain Area

The total forest loss area in Jiangxi Province during 1986–2019 was 18 697.79 km^2, accounting for 15.58% and 24.06% of total forest area in 2019 and 1986, respectively (Fig. 7). The mean annual loss area and rate were 549.94 km^2 and 0.71% (relative to forest area in 1986), respectively. Due to the dynamic changes in forest management and disturbance patterns, forest loss area showed a large interannual variation from 1986 to

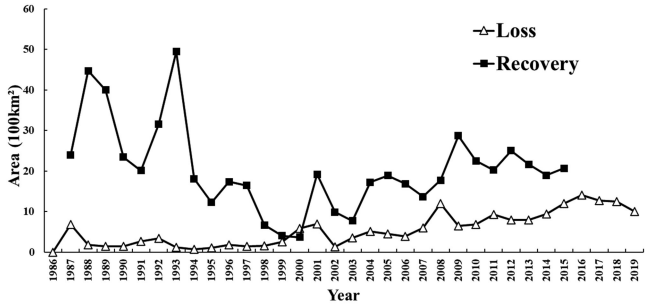

Fig. 7. Interannual variations in total forest loss and gain area (100 km^2) during 1986–2019 in Jiangxi Province. Note: the detection of forest gain during 2016–2019 is not included, due to the long forest recovery or regrowth period and the <5 years' period after 2016 is not enough for an accurate detection.

2019. Annual forest loss area was lower than 300 km^2, and kept no obvious change trend during 1986–2000, while it suddenly increased during 2000 and 2001, reaching 599.22 and 677.00 km^2, respectively. Forest loss area showed an increasing trend from 2002 to 2019, with the highest loss area in 2016 (1398.98 km^2), 2017 (1245.77 km^2), and 2018 (1222.78 km^2), accounting for 1.56%, 1.39%, and 1.36%, respectively, of the total forest land area. The most rapid increasing rate of forest loss area occurred during 2009–2016 after the reform of collective forest tenure was fully implemented in 2008. It is interesting to notice that forest loss area in 2008 was very high and almost the same with that during 2017–2018. A declining trend was seen from 2016 to 2019, implying a stabilizing or declining loss area in future. The forest net loss in Jiangxi Province was caused by land conversion from forests to nonforests, dominated by the conversions to cropland and urban area. Compared with the forest area in 1986 and 2019, the net loss area was 3394.31 km^2, accounting for 18.15% of the total forest loss area. This indicated that over 81.85% of total loss area has been reforestated during the study period.

The total forest gain area during 1986–2015 was 60 387.53 km^2, and the net gain area was 45 656.96 km^2, with a mean annual increasing rate of 1.70% (Fig. 7). The net gain forest area was significantly more than the net loss area. Total forest gain area showed a generally declining trend and a larger interannual variation as compared with forest loss area. Forest gain detections were generally delayed for several years based on the LandTrendr algorithm due to the forest regrowth or recovery generally took several years in the study region, which may greatly affect the actual interannual variation patterns.

C. Spatial Patterns in Forest Loss and Gain Area

Due to various and frequent disturbance events, forest loss and gain frequently and widely occurred in Jiangxi Province during 1986–2019 (Fig. 8). Forest loss areas were generally located surrounding the area with intensive human activities, such as the human settlement regions and the paved roads. These forest loss areas were mainly due to harvesting for timbers and the land use change from forest to urban lawn or urban impervious surfaces. Among the all forest loss areas, about 1.2% have experienced

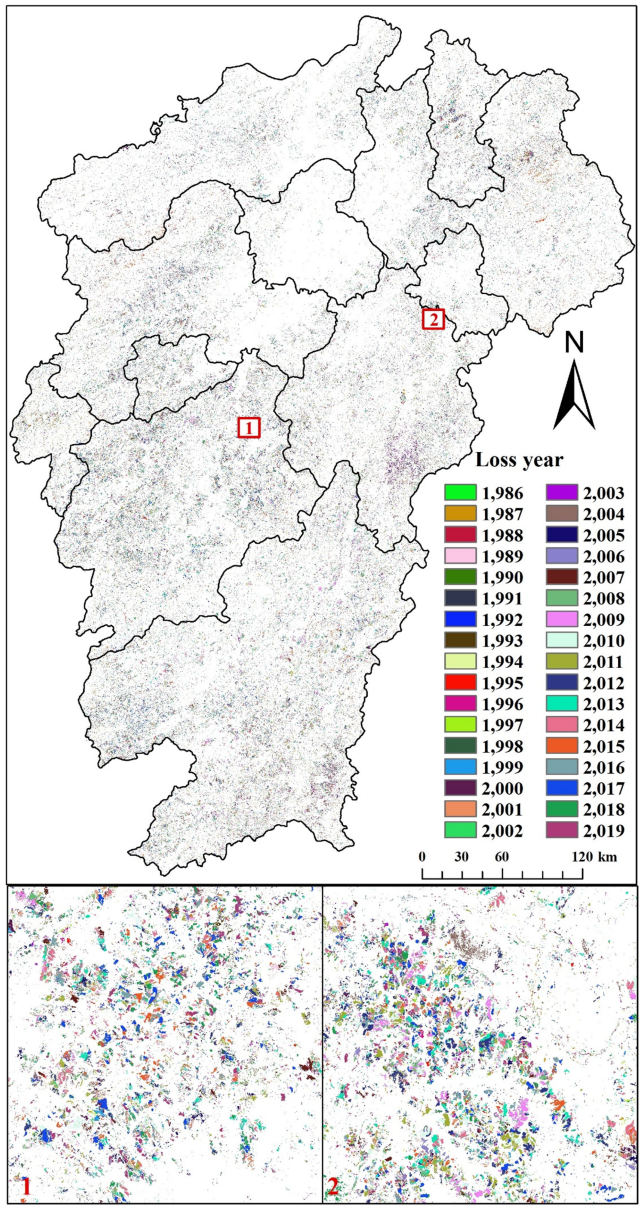

Fig. 8. Spatial distributions in forest loss area and timing during 1986–2019 in Jiangxi Province.

2–3 times of loss during 1986–2019 due to frequent disturbance. From the regular patterns of border shapes, we found that most of the detected forest loss areas were sourced from clearcut. Forest loss areas were generally patchy and densely distributed, while forest gain areas were more scattered and fragmented (Fig. 9). Except for the forest gains from the temporary loss areas, most of the left forest gain areas occurred at the fringes of forest land during 1986–2015.

To look closer at the spatial patterns, the pixel level of forest loss and gain area was further aggregated to city level (Fig. 10). For different cities in Jiangxi Province, the total forest loss area was larger in the cities with higher forest area, such as Ganzhou (forest area: 32 286 km^2; total loss: 5438 km^2; net loss: 2124 km^2), Ji'An (forest area: 17 933 km^2; total loss: 3981 km^2; net

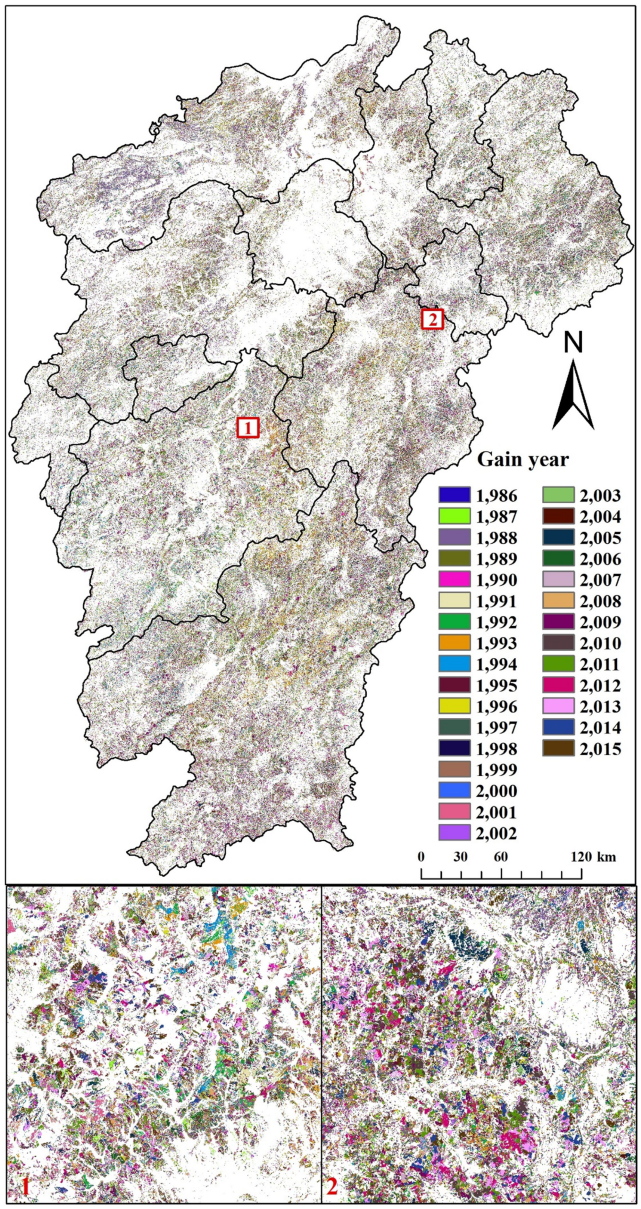

Fig. 9. Spatial distributions in forest gain area during 1986–2015 in Jiangxi Province. Note: the detection of forest gain during 2016–2019 is not included, due to the long forest recovery or regrowth period and the <5 years' period after 2016 is not enough for an accurate detection.

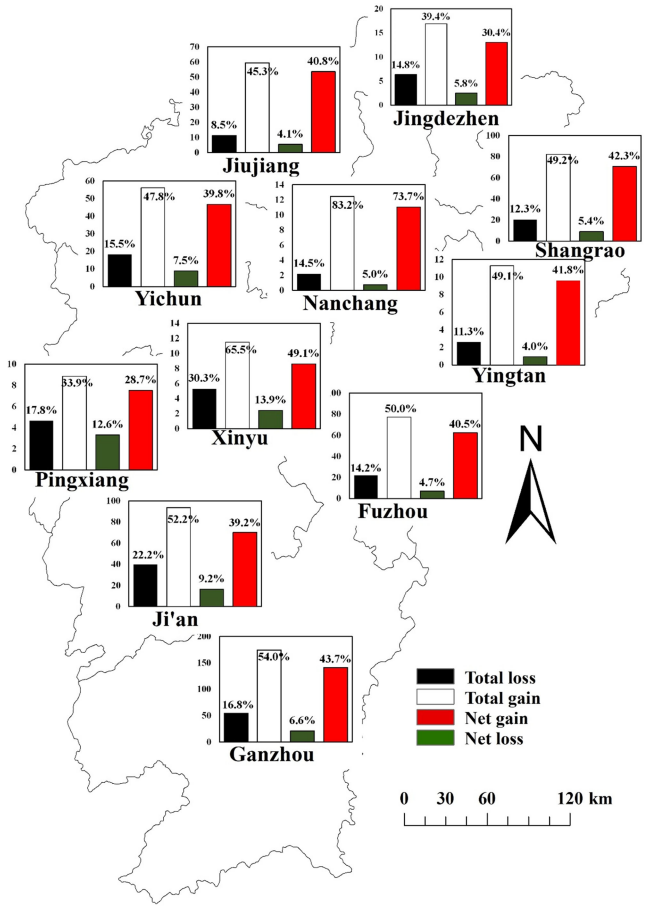

Fig. 10. Total loss, net loss, total gain, net gain area, and their proportions to forest area in different cities of Jiangxi Province during 1986–2019. Note: *Y*-axis is the area (km^2), and the numbers above the bars are the percentage of gain/loss area accounting for the total forest area in 2019.

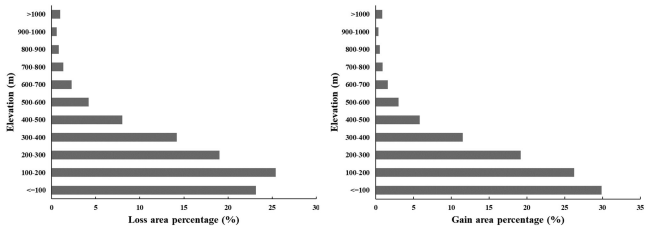

Fig. 11. The frequency (%) distributions of forest total loss area and net gain area along an elevation gradient in Jiangxi Province.

loss: 1651 km^2), and Fuzhou (forest area: 15 427 km^2; total loss: 2193 km^2; net loss: 719 km^2) cities. The highest forest loss fraction was located in Xinyu (total loss: 30.3%; net loss: 13.9%), Ji'An (total loss: 22.2%; net loss: 9.2%), and Pingxiang (total loss: 17.8%; net loss: 12.6%). Compared with other cities, Xinyu and Pingxiang cities had relatively smallest forest area of 1755 and 2613 km^2, respectively. The city level forest gain patterns were slightly different from the forest loss. Ganzhou, Ji'An, Shangrao, and Fuzhou cities had the highest total and net gain forest area, and Nanchang (73.7%), Xinyu (49.1%), and Ganzhou (43.7%) had the highest net gain forest fraction. The different forest loss and gain patterns among these cities were mainly caused by the differences in the city-level economic growth rate, forest management policies, and disturbance intensity.

Accessibility is one of the most important factors that affect the human interferences of forests in the mountainous and hilly Jiangxi Province. The analysis indicated that the spatial distribution patterns of forest loss and gain were significantly correlated with the elevation. Both loss and gain area declined with increasing elevation (Fig. 11). Over 67.58% and 75.28% of the total loss and net gain areas were distributed in the area with elevation below 300 m, while the forest fraction distributed

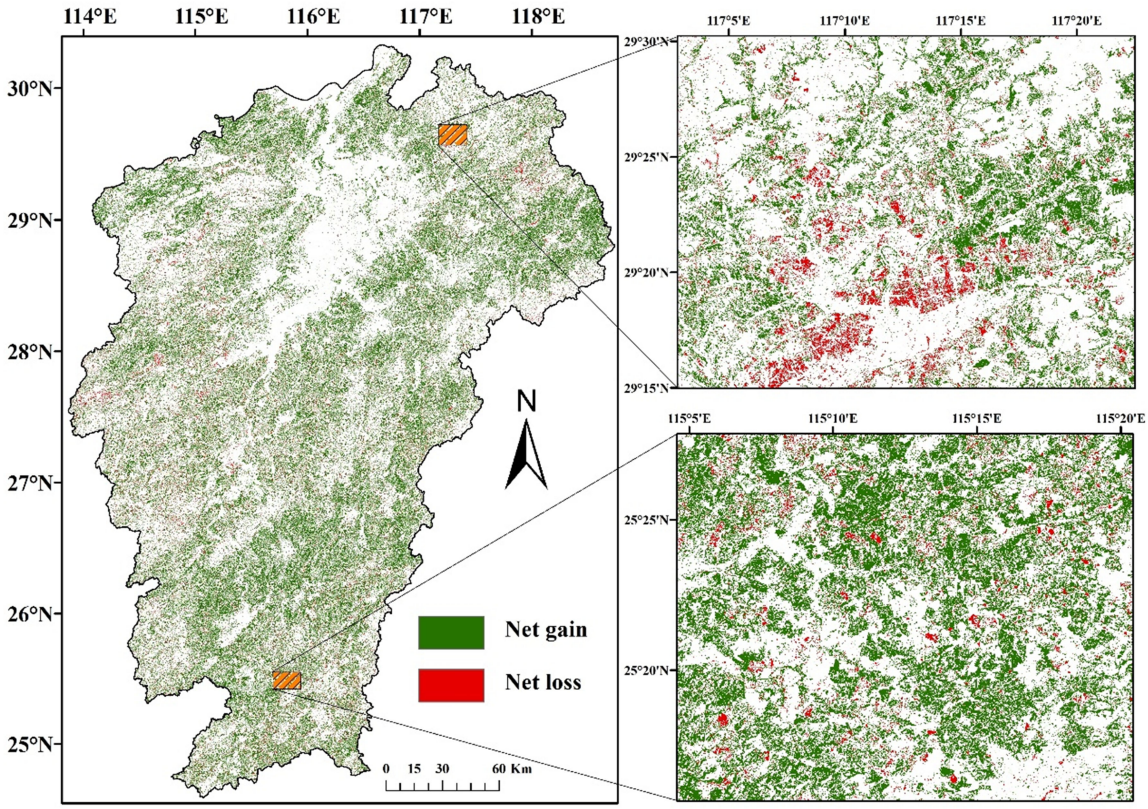

Fig. 12. Net gain and loss of forest cover from 1986 to 2019 in Jiangxi Province.

below 300 m is only 56.26%. This indicated a preference to the management and disturbance at the lower elevation forests.

D. Net Forest Cover Changes From 1986 to 2019

Based on the forest gain and loss data, we calculated the overall net changes in forest cover in Jiangxi Province from 1986 to 2019. The persistent forest gain area was 60 387.53 km^2, and the persistent loss area was 3394.31 km^2, with a net increase of 45 656.96 km^2, which accounted for 38.17% and 57.70% of the forest area in 2019 and 1986, respectively. The forest coverage in Jiangxi Province increased from 47.41% in 1986 to 61.18% in 2019. The very low total loss area and high net gain area indicated that forests in Jiangxi Province were in a recovery or protective utilization mode during 1986–2019. The net loss areas were mainly due to land use change from forest to human settlement areas or to cropland, and mostly distributed close to the urban area or the edges of the forest lands (Fig. 12).

IV. Discussion

A. Comparisons With Other Data Sources

Our detected forest area in Jiangxi Province increased from 79 123.76 km^2 in 1986 to 119 622.55 km^2 in 2019, with a net gain of 40 498.79 km^2 and an increase rate of 51.18%. This is slightly higher than the net gain reported by the NFRIs, which estimated the forest area during 1984–1988 (third NFRI) and 2014–2018 (ninth NFRI) was 72 104 km^2 (has converted from 30% canopy coverage forest to the 20% canopy coverage forest area according to [7] and 102 102 km^2, respectively, with a net forest gain of 29 998 km^2 and increase rate of 41.60%. Our estimated forest loss area was greatly lower than the data reported by the 2004–2008 NFRI, where NFRI reported a large loss area from forest insect & disease. However, our reported loss area was comparable with the data during 2009–2013 and 2014–2018 (Fig. 13). The gap was mainly resulted from the underestimation of the tree loss due to scattered disturbance events such as forest insect & diseases. The 30 m spatial resolution Landsat images can only monitor the disturbance events at area of greater than 900 m^2, but most forest insect & disease events only caused scattered or smaller scale tree death, which could result in the underestimation.

The GFC product [40] was the first and mostly widely used forest disturbance and recovery dataset at middle spatial resolution (30 m). Although the selected few validation forest loss locations from the GFC product matched well with our generated forest loss locations, the interannual and spatial variations of forest loss area were greatly different between these two products (Fig. 14). For total loss area, our results indicated 15 088 km^2 forest losses during 2001–2019 in Jiangxi Province, but estimation from the GFC product was 12 744 km^2, significantly lower than our results. For the interannual variation patterns, both datasets were similar, but there existed significant differences in some

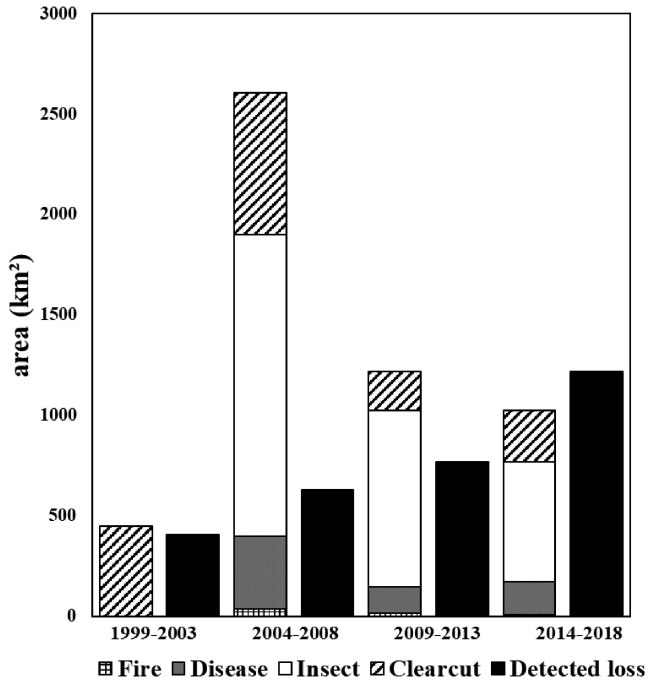

Fig. 13. Mean annual forest loss area detected in our study and the NFRIs (data source: http://forest.ckcest.cn/zh/lytjsjfx.html). Note: the loss area of forest insect and diseases was calculated by multiplying the infected area with the damage rate.

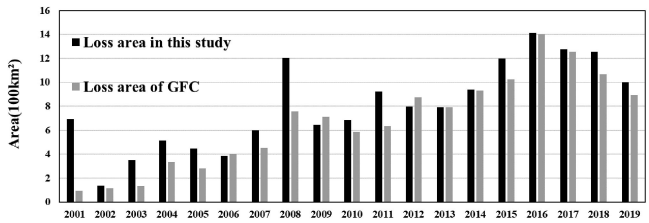

Fig. 14. Comparisons for detected forest loss area (100 km^2) from our study and the global forest change product [40].

years. For example, the GFC product estimated significantly lower forest loss area in 2001–2005, 2008, and 2011. For the spatial distribution patterns, our results matched better than the GFC product as compared with the observed forest loss polygons from the LFMI (Fig. 15). The GFC product lost some forest loss areas, which may be one of the reasons causing significantly lower loss area in some years as compared with our results. For forest gain, the GFC product estimated forest gain area of 1538.4 km^2 during 2001–2012, while our estimation was 6870.4 km^2. During the sixth (1999–2003) and eighth (2009–2013) NFRIs, the forest area in Jiangxi Province was 93 139 and 100 181 km^2, respectively, increased by about 7042 km^2 during 2001–2012. Our estimation is closer to the NFRIs data. The GFC product has been criticized for the lack of enough validations using national inventory data and local forest inventory sample plots [56], while our study not only covered a longer period from 1986–2019 but also well-trained the integrative detection algorithms and extensively validated the detected results.

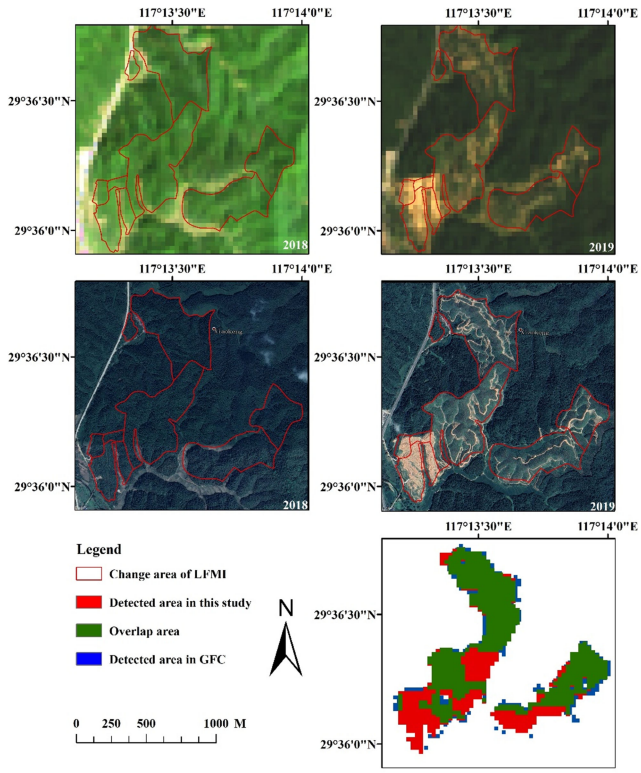

Fig. 15. Comparisons of the detected forest loss polygons in this article with the LFMI inventory data and the global forest change product (GFC; [40]). (a) 2018 Landsat OLI8 images. (b) 2019 Landsat OLI8 images. (c) 2018 high-resolution image from Google Earth. (d) 2019 high-resolution image from Google Earth. (e) Overlay of our classified loss area with global forest change product.

B. Impacts From Forestry Policies, Management, and Disturbance Events

Many studies [57], [58] have indicated that forest cover change is best explained by multiple factors acting synergistically rather than by single-factor causation. Historically, most changes in forest cover were resulted from human activities [59], [60], so the impact of forestry policies and forest management practices on forest changes cannot be ignored. The proportion of forestry sector Gross Domestic Product (GDP) to the total GDP in Jiangxi Province was continuously increasing from 6.61% in 1998 to 20.85% in 2017[3], indicating the increasing importance of forestry in the economic growth of Jiangxi Province. This further resulted in the more intensive human management on the forest land for seeking more forest products and economic returns.

The interannual variation patterns of forest loss area were primarily owing to the interactive effects of forestry policies and forest management practices. The "Law of the People's Republic of China on Forestry" was first enacted and implemented by the central government in 1984 and followed it, the governmental further put forward the polices such as "Guidelines for Preventing Illegal Logging in the Collective Forests of Southern China"

[3][Online]. Available: http://forest.ckcest.cn/sd/si/zglyzcz.html

(1987), "Forest Harvesting and Regeneration Guideline" (1987), and "Management Guidelines for Closed Mountain for Natural Forest Recovery" (1988) [61]. These polices have effectively prevented or reduced the illegal or unplanned forest logging, and resulted in the lower forest loss area in Jiangxi Province during 1986–2000 (Fig. 7). Jiangxi Province is one of the trial regions for the forestry policy "The Reform of Collective Forest Tenure" in 2003, which began to allow households and private companies to own and manage forest land, and expanded the household's land use rights to include transferring, inheriting, and mortgaging its forestland, in addition to access and management [62]. In 2008, this policy was proved effective and was approved to implement across the entire China. Under the supports of this policy, forest logging area in the timberland or commercial forest land has increased since 2003 and reached the highest in 2008.

In addition, many afforestation/reforestation programs in Jiangxi Province have been carried out under the supports of the NFCP and the grain-to-green program polices [61], resulting in rapid increases in planted forest area since 1984, which is proved by the increasing forest cover from 35.94% (the third NFRI; 1984–1988), 40.35% (the fourth NFRI; 1989–1993) to 53.37% (the fifth NFRI; 1994–1998). The forest rotation age is generally 20–30 years for the evergreen needleleaf plantations in Jiangxi Province. With more commercial forest areas reached maturity for harvesting, the timberlands planted in the early 1980s have been continuously harvested since the early of 2000s, and thus caused a continuous increasing forest loss area and reached the highest in 2016 (Fig. 7). The forest loss area slightly dropped off after 2016 since the forest area suitable for logging was declining. In addition, with the implementations of the forestry policies "Guidelines on Strict Natural Forest Protection" in 2015 and the amended "Law of the People's Republic of China on Forestry," the forest land reserved for the functional group of commercial forest was also declined.

In addition to forestry policies and forest management, extreme disturbance events, such as the extreme winter freezing disaster in 2008 and the recorded most severe drought events in 1991, 2000, 2003, 2007, 2011, and 2019, could have also caused large forest loss area [5], [63]. There is a delaying effect for the drought impacts, so the drought events may also cause forest mortality in the following several years. The high forest loss area in 1992, 2000, 2001, and 2004 may be partially due to the drought events in 1991, 2000, and 2003, respectively. Furthermore, the forest insects and diseases, such as the pine wood nematode disease (*Bursaphelenchus xylophilus*) and long-horned beetle (*Cerambycidae*) have been reported to cause large area mortality of *P. massoniana* forests in Jiangxi Province during the recent decade[4].

C. Uncertainties and Outlooks

The LandTrendr algorithms require a large number of Landsat images within a year to derive forest gain and loss, and the effective integration of all available Landsat images is the advantage and superiority of LandTrendr algorithms over other disturbance and recovery algorithms [24], [41], [53]. The fewer available cloud-free Landsat image scenes before 2000 might cause larger uncertainties in the classified forest gain and loss during 1986–2000, resulting in an underestimation. In addition, the middle spatial resolution (30 m) of the Landsat images may result in the ignoring of the effects from smaller scale disturbance events, such as the impacts of hurricane/typhoon, partial harvesting, and insects & diseases, which could result in some underestimations in forest loss area. Partial harvesting by household use of timber (for building) and firewood (for cooking) occurred frequently before 2000 and gradually decreased with the rapid economic growth, and the spreading of electric and gas cookers in Jiangxi Province. Forest recovery and regrowth after loss is a relatively long period, and the detection of forest gain often need take several years; therefore, the detected forest gain area in this year may be actually resulted from the previous several years, which could cause some uncertainties in the annual variation patterns in forest gain area.

In addition, our current algorithms integrated LandTrendr with RF can only monitor the stand-replacing (complete loss of forest stands) disturbance events. As indicated in our study, there are many disturbance events such as forest insect and disease outbreaks in Jiangxi Province, which mostly cause nonstand replacing fractional or small area (less than 900 m^2) loss of trees. These nonstand replacing disturbances cannot be effectively classified using our algorithms [19], [41], [64], [65]. Fortunately, Jarron *et al.* [33] and Coops *et al.* [65] have developed a composite change method to detect the non-standing-replacing disturbances. In addition, Zhu *et al.* [66] developed a COLD method to detect disturbances for all land cover types and for fractional disturbance events, without sample plot data for training this algorithm. In future, we will apply these methods to further classify the fractional forest loss or gain rates after disturbance events.

Unlike the intensively managed forests in the southern United States and other countries in Europe (e.g., Finland), clearcut is the main forest harvesting mode in Jiangxi Province and many other China's provinces, and almost no large-scale partial harvesting at mature age. This makes it easier for the LandTrendr algorithms to detect stand-replacing forest loss area resulted from forest harvesting, and our validation using plot-level and GFC product has also proved the effectiveness of our classification processes. As compared with the LandTrendr algorithm solely based on NBR index [13], [24], [27], [53], we used a secondary classification approach by integrating the most important six indices and spectral bands into the LandTrendr and RF classifier [41], [64]. This method is proved to be more effective in our study, and thus this combined approach can be effectively applied to estimate forest disturbance and recovery in the entire China.

Although there are some uncertainties, our study results are one of the first few attempts to assess the spatial and temporal patterns of forest disturbance and subsequent recovery at provincial level. As a pilot study region, our goal is to extend our study approach to the entire subtropical China, where is the main timberland base in China at present [3]. In addition, the forests are intensively and frequently managed and disturbed in this region due to the changes in forestry policies and projects

[4][Online]. Available: http://forest.ckcest.cn/sd/si/zgslbh.html

such as the reform of collective forest tenure and several afforestation/reforestation projects [16], [61]. These resulted in large-area and rapid forest cover change in this region. Thus, a long-term spatial-explicit disturbance and recovery dataset is necessary for assessing forest resources, global change impacts, and greenhouse gas emissions in China.

V. Conclusion

Based on 30 m Landsat archive and cloud-based computation platform GEE, we used LandTrendr temporal segmentation algorithm and the RF classifier to map forest disturbance and recovery from 1986 to 2019 in the subtropical China. The large numbers of training sample data can greatly improve the performance of RF classifier. The detected forest loss and gain area was extensively validated against a lot of plot-level sample data and achieved high overall accuracy and Kappa Coefficient, suggesting a high quality of the derived forest loss and gain datasets. The mean annual forest loss and gain rates were 0.71% and 1.70%, respectively, relative to the forest area in 1986, suggesting forests in Jiangxi Province were in a recovery or protective utilization mode during 1986–2019. The results clearly revealed forest change progress, both spatially and temporally, as well as the effects of forest management policy changes on forest dynamics from 1986 to 2019. Our dataset supplies detailed information about the temporal and spatial changes of forests in Jiangxi Province, and provides more change details at annual intervals to fill in gaps missed by other products with longer time intervals. More than 34 years of monitoring make our data helpful to understand the characteristics and mechanisms of forest change in Jiangxi Province. Timely and transparent monitoring of forest change is crucial for implementing more effective forest-based climate mitigation policies and for tracking the progress of country-based climate-mitigation targets [67].

Acknowledgment

The authors would like to thank the cloud computing platform of Google Earth Engine to access and process the Landsat images, and the open access of Global Forest Change product. We also greatly appreciate Dr. Shilong Piao and Dr. Yuan Zhang from Peking University for providing the 1-km spatial resolution forest age dataset.

References

[1] E. Meijaard *et al.*, "People's perceptions about the importance of forests on borneo," *PloS One*, vol. 8, 2013, Art. no. e73008.
[2] C. Chen *et al.*, "China and India lead in greening of the world through land-use management," *Nat. Sustainability*, vol. 2, pp. 122–129, 2019.
[3] Z. Yu *et al.*, "Mapping forest type and age in China's plantations," *Sci. Total Environ.*, vol. 744, 2020, Art. no. 140790.
[4] C. Zhang *et al.*, "Mapping forest stand age in China using remotely sensed forest height and observation data," *J. Geophys. Res.: Biogeosci.*, vol. 119, pp. 1163–1179, 2014.
[5] P. Zhang *et al.*, "Global warming and droughts aggravates forest damage resulting from pests and diseases in Jiangxi province," *Acta Ecologica Sinica*, vol. 37, pp. 639–649, 2017.
[6] J. Fang, Z. Guo, H. hu, T. Kato, H. Muraoka, and Y. Son, "Forest biomass carbon sinks in east Asia, with special reference to the relative contributions of forest expansion and forest growth," *Global Change Biol.*, vol. 20, pp. 2019–2030, 2014.
[7] J. Fang, Z. Guo, S. Piao, and A. Chen, "Terrestrial vegetation carbon sinks in China, 1981–2000," *Sci. China Ser. D: Earth Sci.*, vol. 50, pp. 1341–1350, 2007.
[8] Y. Pan *et al.*, "A large and persistent carbon sink in the world's forests," *Science*, vol. 333, pp. 988–993, 2011.
[9] X. Wei and J. Blanco, "Significant increase in ecosystem C can be achieved with sustainable forest management in subtropical plantation forests," *PloS One*, vol. 9, 2014, Art. no. e89688.
[10] S. Piao *et al.*, "The carbon balance of terrestrial ecosystems in China," *Nature*, vol. 458, no. 7241, pp. 1009–1013, 2009.
[11] G. Yu *et al.*, "High carbon dioxide uptake by subtropical forest ecosystems in the east Asian monsoon region," in *Proc. Nat. Acad. Sci. United States Amer.*, 2014, pp. 4910–4915.
[12] W. Liu *et al.*, "The influence of disturbance and conservation management on the greenhouse gas budgets of China's forests," *J. Cleaner Prod.*, vol. 261, 2020, Art. no. 121000.
[13] W. Shen and M. Li, "Mapping disturbance and recovery of plantation forests in southern China using yearly Landsat time series observations," *Acta Ecologica Sinica*, vol. 37, no. 5, pp. 1438–1449, 2017.
[14] L. Zhong, Y. Chen, and X. Wang, "Forest disturbance monitoring based on time series of Landsat data," *Scientia Silvae Sinicae*, vol. 56, no. 5, pp. 80–88, 2020.
[15] X. Wang, F. Yang, X. Gao, W. Wang, and X. Zha, "Evaluation of forest damaged area and severity caused by Ice-snow frozen disasters over southern China with remote sensing," *Chin. Geographical Sci.*, vol. 29, no. 3, pp. 405–416, 2019.
[16] W.S. Zeng, "The national forest inventory in China: History-results-international context," *Forest Ecosyst.*, vol. 2, 2015, Art. no. 23.
[17] C. Xu, "Forest management in China from data of eight forest resources inventories," *Forestry Econ.*, vol. 36, no. 4, pp. 8–11, 2014.
[18] C. Huang, S. Goward, J. Masek, N. Thomas, Z. Zhu, and J. Vogelmann, "An automated approach for reconstructing recent forest disturbance history using dense Landsat time series stacks," *Remote Sens. Environ.*, vol. 114, no. 1, pp. 183–198, 2010.
[19] R. Kennedy, Z. Yang, and W. Cohen, "Detecting trends in forest disturbance and recovery using yearly Landsat time series: 1. Landtrendr—Temporal segmentation algorithms," *Remote Sens. Environ.*, vol. 114, no. 12, pp. 2897–2910, 2010.
[20] S. Obata, P. Bettinger, C. J. Cieszewski, and R.C. Lowe III, "Mapping forest disturbances between 1987–2016 using all available time series Landsat TM/ETM+ imagery: Developing a reliable methodology for Georgia, United States," *Forests*, vol. 11, no. 3, 2020, Art. no. 335.
[21] K. G. Schleeweis *et al.*, "US national maps attributing forest change: 1986–2010," *Forests*, vol. 11, no. 6, 2020, Art. no. 653.
[22] J. Verbesselt, R. Hyndman, G. Newnham, and D. Culvenor, "Detecting trend and seasonal changes in satellite image time series," *Remote Sens. Environ.*, vol. 114, pp. 106–115, 2010.
[23] B. C. Bright, A. T. Hudak, R. E. Kennedy, and A. J. H. Meddens, "Landsat time series and lidar as predictors of live and dead basal area across five bark beetle-affected forests," *IEEE J. Sel. Topics Appl. Earth Observ. Remote Sens.*, vol. 7, no. 8, pp. 3440–3452, 2014.
[24] W. Cohen *et al.*, "Forest disturbance across the conterminous United States from 1985–2012: The emerging dominance of forest decline," *Forest Ecol. Manage.*, vol. 360, pp. 242–252, 2016.
[25] R. Frazier, N. Coops, and M. Wulder, "Boreal shield forest disturbance and recovery trends using Landsat time series," *Remote Sens. Environ.*, vol. 170, pp. 317–327, 2015.
[26] K. Grogan, D. Pflugmacher, P. Hostert, R. Kennedy, and R. Fensholt, "Cross-border forest disturbance and the role of natural rubber in mainland southeast Asia using annual Landsat time series," *Remote Sens. Environ.*, vol. 169, pp. 438–453, 2015.
[27] S. Liu, X. Wei, D. Li, and D. Lu, "Examining forest disturbance and recovery in the subtropical forest region of Zhejiang province using Landsat time-series data," *Remote Sens.*, vol. 9, 2017, Art. no. 479.
[28] Y. Zhang, Y. Yao, X. Wang, Y. Liu, and S. Piao, "Mapping spatial distribution of forest age in China: Map of forest age in China," *Earth Space Sci.*, vol. 4, pp. 108–116, 2016.
[29] A. Banskota, N. Kayastha, M. Falkowski, M. Wulder, R. Froese, and J. White, "Forest monitoring using Landsat time series data: A review," *Can. J. Remote Sens.*, vol. 40, no. 5, pp. 362–384, 2014.
[30] D. Lu, G. Li, and E. Moran, "Current situation and needs of change detection techniques," *Int. J. Image Data Fusion*, vol. 5, no. 1, pp. 13–38, 2014.
[31] R. Kennedy, W. Cohen, and T. Schroeder, "Trajectory-based change detection for automated characterization of forest disturbance dynamics," *Remote Sens. Environ.*, vol. 110, no. 3, pp. 370–386, 2007.

[32] T. Hermosilla, M. Wulder, J. White, N. Coops, and G. Hobart, "Regional detection, characterization, and attribution of annual forest change from 1984 to 2012 using Landsat-derived time-series metrics," *Remote Sens. Environ.*, vol. 170, pp. 121–132, 2015.
[33] L. Jarron *et al.*, "Differentiation of alternate harvesting practices using annual time series of Landsat data," *Forests*, vol. 8, no. 1, 2017, Art. no. 15.
[34] R. Kennedy *et al.*, "Attribution of disturbance change agent from Landsat time-series in support of habitat monitoring in the puget sound region, USA," *Remote Sens. Environ.*, vol. 166, pp. 271–285, 2015.
[35] G. Meigs, R. Kennedy, and W. Cohen, "A Landsat time series approach to characterize bark beetle and defoliator impacts on tree mortality and surface fuels in conifer forests," *Remote Sens. Environ.*, vol. 115, no. 12, pp. 3707–3718, 2011.
[36] J. Diao *et al.*, "Use of vegetation change tracker, spatial analysis, and random forest regression to assess the evolution of plantation stand age in southeast China," *Ann. Forest Sci.*, vol. 77, 2020, Art. no. 27.
[37] L. Zhang, "Forest disturbance monitoring and trend analysis based on time series of Landsat data," Graduation thesis, Key Lab Spatial Data Mining & Inf. Sharing, Ministry Educ., Fuzhou Univ., Fuzhou, China, 2016, p. 61.
[38] X. Y. Guo, "Detecting forest disturbance in northeastern China using remote sensing data," Graduation thesis, Dept. Geographic Sci., Northeast Normal Univ., Changchun, China, 2015, p. 127.
[39] L. Fang, J. Yang, W. Zhang, W. Zhang, and Q. Yan, "Combining allometry and Landsat-derived disturbance history to estimate tree biomass in subtropical planted forests," *Remote Sens. Environ.*, vol. 235, 2019, Art. no. 111423.
[40] M. C. Hansen *et al.*, "High-resolution global maps of 21st-century forest cover change," *Science*, vol. 342, no. 6160, pp. 850–853, 2013.
[41] W. Cohen, Z. Yang, S. Healey, R. Kennedy, and N. Gorelick, "A landtrendr multispectral ensemble for forest disturbance detection," *Remote Sens. Environ.*, vol. 205, pp. 131–140, 2018.
[42] S. Goward *et al.*, "Forest disturbance and North American carbon flux," *EOS Trans. Amer. Geophys. Union*, vol. 89, no. 11, pp. 105–106, 2008.
[43] A. Ahrends *et al.*, "China's fight to halt tree cover loss," in *Proc. R. Soc. B*, vol. 284, no. 1854, 2017, pp. 1–10.
[44] L. Huang, Q. Shao, and J. Liu, "Forest carbon sequestration and carbon sink/source in Jiangxi province," *Acta Ecologica Sinica*, vol. 32, no. 10, pp. 3010–3020, 2012.
[45] L. Dai *et al.*, "Major forest types and the evolution of sustainable forestry in China," *Environ. Manage.*, vol. 48, no. 6, pp. 1066–1078, 2011.
[46] D. Li, C. Zhang, W. Ju, and L. Liu, "Forest net primary productivity dynamics and driving forces in Jiangxi province, China," *Chin. J. Plant Ecol.*, vol. 40, pp. 643–657, 2016.
[47] C. Li *et al.*, "A circa 2010 thirty meter resolution forest map for China," *Remote Sens.*, vol. 6, no. 6, pp. 5325–5343, 2014.
[48] D. J. Hayes, W. B. Cohen, S. A. Sader, and D. E. Irwin, "Estimating proportional change in forest cover as a continuous variable from multi-year MODIS data," *Remote Sens. Environ.*, vol. 112, no. 3, pp. 735–749, 2008.
[49] E. Vermote, C. Justice, M. Claverie, and B. Franch, "Preliminary analysis of the performance of the Landsat 8/OLI land surface reflectance product," *Remote Sens. Environ.*, vol. 185, pp. 46–56, 2016.
[50] S. Foga *et al.*, "Cloud detection algorithm comparison and validation for operational Landsat data products," *Remote Sens. Environ.*, vol. 194, pp. 379–390, 2017.
[51] D. Roy *et al.*, "Characterization of Landsat-7 to Landsat-8 reflective wavelength and normalized difference vegetation index continuity," *Remote Sens. Environ.*, vol. 185, pp. 57–70, 2016.
[52] J. Verbesselt, A. Zeileis, and M. Herold, "Near real-time disturbance detection using satellite image time series," *Remote Sens. Environ.*, vol. 123, pp. 98–108, 2012.
[53] R. E. Kennedy, Z. Yang, W. B. Cohen, E. Pfaff, J. Braaten, and P. Nelson, "Spatial and temporal patterns of forest disturbance and regrowth within the area of the northwest forest plan," *Remote Sens. Environ.*, vol. 122, pp. 117–133, 2012.
[54] S. Saura, "Effects of minimum mapping unit on land cover data spatial configuration and composition," *Int. J. Remote Sens.*, vol. 23, no. 22, pp. 4853–4880, 2002.
[55] S. Stehman, "Selecting and interpreting measures of thematic classification accuracy," *Remote Sens. Environ.*, vol. 62, no. 1, pp. 77–89, 1997.
[56] R. Tropek *et al.*, "Comment on "High-resolution global maps of 21st-century forest cover change"," *Science*, vol. 344, no. 6187, 2014, Art. no. 981.
[57] K. Bawa and S. Dayanandan, "Socioeconomic factors and tropical deforestation," *Nature*, vol. 386, no. 6625, pp. 562–563, 1997.
[58] D. Southgate, R. Sierra, and L. Brown, "The causes of tropical deforestation in Ecuador: A statistical analysis," *World Develop.*, vol. 19, no. 9, pp. 1145–1151, 1991.
[59] R. Houghton, "Tropical deforestation and atmospheric carbon dioxide," *Climatic Change*, vol. 19, pp. 99–118, 1991.
[60] W. Meyer and B. L. Turner Ii, "Human population growth and global land-use/cover change," *Annu. Rev. Ecol. Syst.*, vol. 23, no. 1, pp. 39–61, 1992.
[61] D. Pan, H. Chen, and F. B. Kong, "The evolution of forestry policies since 1949: A quantitative analysis based on 283 texts of forest-related normative policy documents," *Chin. Rural Econ.*, vol. 451, no. 7, pp. 89–108, 2019.
[62] P. Qin, F. Carlsson, and J. T. Xu, "Forest tenure reform in China: A choice experiment on farmers' property rights preferences," *Land Econ.*, vol. 87, no. 3, pp. 473–487, 2011.
[63] Y. Liu, H. Wang, and W. Ju, "Characteristics of drought effects on forest productivity in Jiangxi province," *J. Natural Disasters*, vol. 25, no. 3, pp. 67–77, 2016.
[64] W. Cohen, S. Healey, Z. Yang, Z. Zhu, and N. Gorelick, "Diversity of algorithm and spectral band inputs improves Landsat monitoring of forest disturbance," *Remote Sens.*, vol. 12, 2020, Art. no. 1673.
[65] N. Coops, C. Shang, M. Wulder, J. White, and T. Hermosilla, "Change in forest condition: Characterizing non-stand replacing disturbances using time series satellite imagery," *Forest Ecol. Manage.*, vol. 474, 2020, Art. no. 118370.
[66] Z. Zhu *et al.*, "Continuous monitoring of land disturbance based on Landsat time series," *Remote Sens. Environ.*, vol. 238, pp. 111–116, 2019, Art. no. 111116.
[67] G. Ceccherini *et al.*, "Abrupt increase in harvested forest area over Europe after 2015," *Nature*, vol. 583, no. 7184, pp. 72–77, 2020.

Jianwen Hua received the B.S. degree in forestry from Zhejiang A&F University, Hangzhou, China, in 2017. He is currently working toward the M.S. degree in remote sensing at the College of Environmental and Resource Sciences, Zhejiang A&F University, Hangzhou, China.

His research interests include remote sensing detections of disturbance events and geospatial data analysis.

Guangsheng Chen received the Ph.D. degree in forestry from Auburn University, Auburn, AL, USA, in 2010.

He is currently a Full Professor with the College of Environmental and Resource Sciences, Zhejiang A&F University, Hangzhou, China. He has authored four book chapters and more than 80 peer-review papers, including PNAS, *Nature, Global Change Biology, Earth System Science Data, Global Biogeochemical Cycles*, *Journal of Geophysical Research, Remote sensing*, etc. His research interests include vegetation remote sensing, ecosystem modeling, and geospatial big data analysis.

Prof. Chen is a member of Ecological Society of America and American Geophysical Union.

Lin Yu received the B.S. degree in broadcasting from Central Radio and Television University, Beijing, China, in 2005.

She is currently an Assistant Engineer with Bureau of Agriculture and Rural Affairs of Lin'An District, Hangzhou, China. She is the Chief of Personnel Section at the Bureau of Agriculture and Rural Affairs of Lin'An District. Her research interests include degraded forest land restoration and improvement, and dissemination of new technology in forestry.

Qing Ye received the Ph.D. degree in agrometeorology from China Agricultural University, Beijing, China, in 2013.

He is an Associate Professor in applied meteorology with the College of Forestry, Jiangxi Agricultural University, Nanchang, China. He has authored eight books and over 50 peer-review papers. His research interests include the analysis and modeling of climate change effects on forest and cropland productivity.

Hongbo Jiao received the M.S. degree in forestry from the College of Forestry, Jiangxi Agricultural University, Nanchang, China, in 2009.

He is currently a Researcher and Technician with the Forestry Industry Development Administration, Xinyu, China. His research interests include forest resource management, assessment and protection, and dissemination of new technology in forestry.

Xifang Luo received the master's degree in forestry from Chinese Academy of Forestry, Beijing, China, in 2004.

He is currently a Full Professor and an Engineer with the East China Forest Inventory and Planning Institute, National Forestry and Grassland Administration, Hangzhou, Zhejiang. He is currently the Director of the second division with the Forest Planning and Design Bureau, East China Forest Inventory and Planning Institute of National Forestry and Grassland Administration. His research interests include forest resource monitoring and assessment, and forest survey planning and design.